# Final Report

# GaAs Shallow-Homojunction Solar Cells

J.C.C. Fan



30 June 1981

Prepared for National Aeronautics and Space Administration
under Contract NAS C-16366-D by

Lincoln Laboratory
MASSACHUSETTS INSTITUTE OF TECHNOLOGY
LEXINGTON, MASSACHUSETTS

Technical Report Documentation Page

| 1. Report No. | 2. Government Accession No. | 3. Recipient's Catalog No. |
|---|---|---|
| NASA CR-165579 | | |

| 4. Title and Subtitle | 5. Report Date |
|---|---|
| GaAs SHALLOW-HOMOJUNCTION SOLAR CELLS | 30 June 1981 |
| | 6. Performing Organization Code |
| 7. Author(s) | 8. Performing Organization Report No. |
| John C.C. Fan | |
| 9. Performing Organization Name and Address | 10. Work Unit No. (TRAIS) |
| Lincoln Laboratory, M.I.T.<br>P.O. Box 73<br>Lexington, MA 02173 | 11. Contract or Grant No.<br>NAS C-46566-D |
| | 13. Type of Report and Period Covered |
| 12. Sponsoring Agency Name and Address | Contractor Report |
| National Aeronautics and Space Administration<br>Washington, DC 20546 | 14. Sponsoring Agency Code |

15. Supplementary Notes

16. Abstract

With the objective of demonstrating the feasibility of fabricating space-resistant, high-efficiency, light-weight, low-cost GaAs shallow-homojunction solar cells for space application, this program has been addressing the material preparation of ultrathin GaAs single-crystal layers, and the fabrication of efficient GaAs solar cells on bulk GaAs substrates. Considerable progress has been made in both areas, and conversion efficiency about 16% AMO have been obtained using anodic oxide as a single-layer antireflection coating. Our computer design shows that even better cells can be obtained with double-layer antireflection coating. Ultrathin, high-efficiency solar cells have also been obtained from GaAs films prepared by the CLEFT process, with conversion efficiency as high as 17% at AM1 from a 10-μm thick GaAs film. A new organometallic CVD has been designed and constructed.

| 17. Key Words | 18. Distribution Statement |
|---|---|
| Antireflection coating<br>GaAs solar cells<br>Space applications<br>CVD growth processes<br>Device fabrication techniques<br>Computer cell modeling | Unclassified - Unlimited |

| 19. Security Classif. (of this report) | 20. Security Classif. (of this page) | 21. No. of Pages | 22. Price* |
|---|---|---|---|
| Unclassified | Unclassified | 56 | |

*For sale by the National Technical Information Service, Springfield, Virginia 22161

## ABSTRACT

With the objective of demonstrating the feasibility of fabricating space-resistant, high efficiency, light-weight, low-cost GaAs shallow-homojunction solar cells for space application, this program has been addressing the material preparation of ultrathin GaAs single-crystal layers, and the fabrication of efficient GaAs solar cells on bulk GaAs substrates. Considerable progress has been made in both areas, and conversion efficiency abo t 16% AMO have been obtained using anodic oxide as a single-layer antireflection coating. Our computer design shows that even better cells can be obtained with double-layer antireflection coating. Ultrathin, high-efficiency olar cells have also been obtained from GaAs films prepared by the CLEFT process, with conversion efficiency as high as 17% at AM1 from a 10-μm thick GaAs film. A new organometallic CVD has been designed and constructed.

CONTENTS

## ACKNOWLEDGMENTS

This work was performed with the collaboration of C. O. Bozler, R. L. Chapman, F. M. Davis, R. P. Gale, R. W. McClelland, B. J. Palm, and G. W. Turner. The technical assistance of M. K. Connors, G. H. Foley, and W. L. McGilvary is sincerely appreciated.

# GaAs SHALLOW-HOMOJUNCTION SOLAR CELLS

The objective of this program is to develop CVD growth processes and device fabrication technique so as to produce space-resistant, high efficiency, light-weight, low-cost GaAs shallow-homojunction solar cells.

## I. INTRODUCTION

Although Si solar cells have been extensively used in space, GaAs cells are now emerging as promising candidates for space applications with a number of potential advantages over Si cells. Since GaAs absorbs sunlight very effectively, solar cells made of GaAs can be much thinner than those made of Si. Figure 1 plots the normalized photocurrent at AM0 as a function of thickness for GaAs and Si. For GaAs a 2-μm-thick layer can generate over 90% of the maximum photocurrent produced by an infinite thickness. Silicon, however, requires a layer over 100 μm thick to achieve the same ratio. Because of the difference in absorption, GaAs cells should also exhibit less radiation damage in space since damage generated more than a few absorption lengths beneath the surface should have little effect on photocurrent collection.[1] In addition, the theoretical conversion efficiency is higher for GaAs than for Si (see Ref. 2), and GaAs cells operate better than Si cells at elevated temperatures[2] and high solar concentrations.[3] Therefore, GaAs cells are very promising candidates for space applications.

By using an $n^+/p/p^+$ shallow-homojunction structure, without a GaAlAs window layer, we have fabricated GaAs solar cells on single-crystal GaAs[4] and Ge[5,6] substrates with conversion efficiency as high as 21% at AM1. The

112408-N

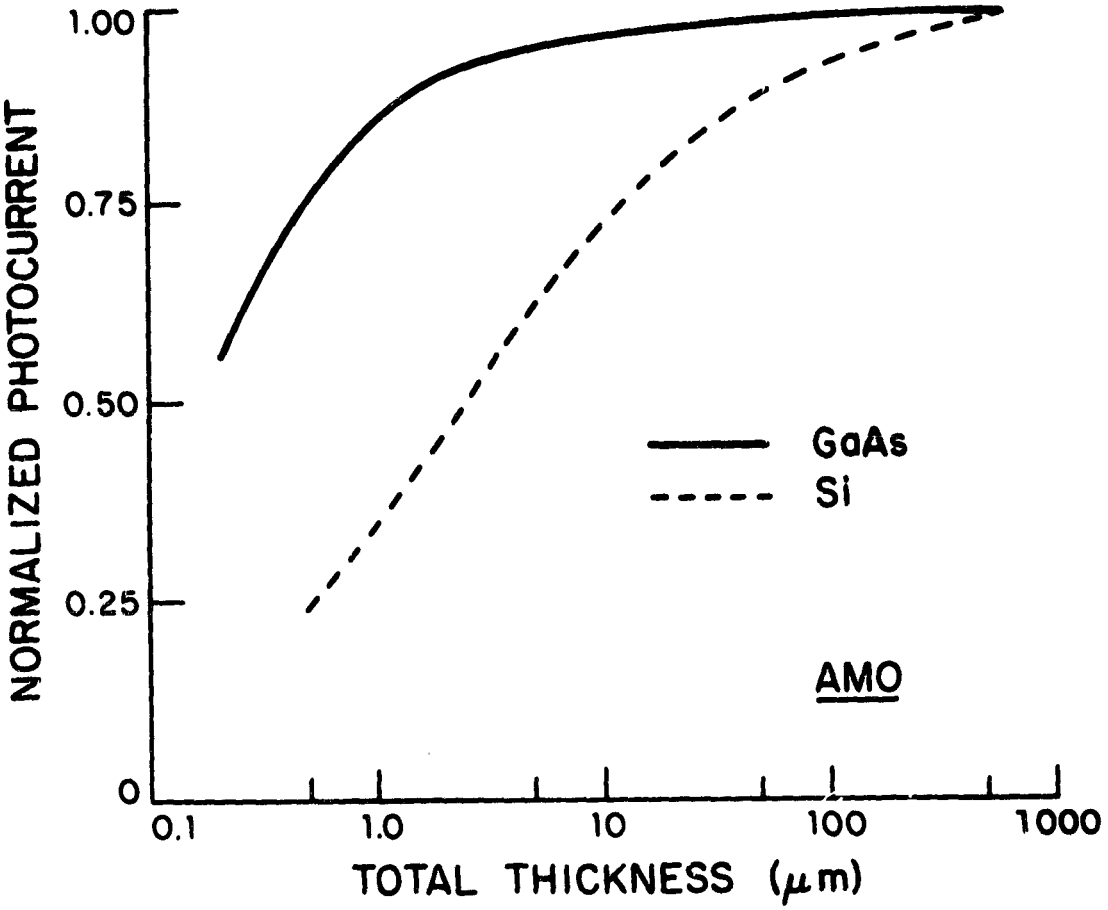


Fig. 1. Normalized photocurrent computed for Si and GaAs as a function of solar cell thickness for AMO.

21% efficient cells on Ge, which have a GaAs epilayer only 4 μm thick, are the most efficient thin-film cells prepared to date. The Ge substrates play a passive role that permits them to be substituted for GaAs substrates without any effect on cell efficiency.

We believe that the $n^+/p/p^+$ configuration is ideally suited for space applications. The heavily doped layers on the front and back surfaces allow easy fabrication of good ohmic contacts. The thin $n^+$ layer is comparable in sheet resistance to the thicker $p^+$ layer in the $p^+/n$ structure of GaAlAs/GaAs heteroface cells,[7] mainly because the majority carriers in the $n^+$ layer are electrons and the electron mobility in GaAs is about 20 times higher than the hole mobility for similarly doped p-layers. This is an important property that makes the shallow-homojunction structure a prime candidate for utilization in concentrator cells. Preliminary results[8] have confirmed that this structure is indeed good for concentrator cells.

The $p^+$ layer in the shallow-homojunction structure facilitates the formation of low-resistance heterojunction contacts to foreign substrates, as demonstrated by the fabrication of GaAs cells on Ge substrates[4] and recently on Ge-coated Si substrates.[9] Furthermore, the $p^+$ layer provides a back-surface field, minimizing recombination losses at the interface with a foreign substrate. Finally, in the shallow-homojunction structure almost all the photocurrent is generated in the p-layer, which normally has a minority-carrier diffusion length (> 20 μm) that is much higher than the solar absorption length (~ 2 μm). Therefore, growth on a foreign substrate can cause a marked reduction in the electron diffusion length in the p-layer

without producing a significant decrease in cell photocurrent. This is confirmed by the observation of a decrease of only 5% in the photocurrent in our GaAs cells on Ge-coated Si substrates, despite the large concentration of dislocations ($\sim 10^7$ cm$^{-2}$) in the p-GaAs layer.[9]

Moreover, the $n^+/p/p^+$ structure is advantageous for monolithic tandem devices because the heavily doped $n^+$ and $p^+$ layers on the front and back surfaces of the GaAs cells allow tunnel junctions to be more easily attained. In addition, degradations in material quality that may result from lattice mismatches in tandem cell structure should not greatly affect the photocurrent.

Because the $n^+$ layer is so thin (< 1000 Å), almost all the electron damage effects will occur in the p layer, where a marked decrease in minority carrier diffusion length can occur without significant reduction in efficiency. Thus, the $n^+/p$ configuration should be very radiation resistant. We have confirmed this superior radiation resistance in a series of experiments using high-energy electron bombardment.[1]

Our $n^+/p/p^+$ structures are grown by chemical vapor deposition (CVD) in an $AsCl_3$-GaAs-$H_2$ system with a vertical fused silica reactor.[5] Comparable cells can be obtained with either a Ga liquid source or GaAs solid source. The CVD technique potentially can be scaled up for mass production. The as-grown thicknesses of $n^+$, p and $p^+$ layers are about 0.15, 2, and 2 μm, respectively. The $n^+$ layer is doped with sulphur to about $5 \times 10^{18}$ cm$^{-3}$, the p layer with zinc to about $10^{17}$ cm$^{-3}$ and the $p^+$ layer with zinc to about $5 \times 10^{18}$ cm$^{-3}$. We have found that cell efficiency is not very sensitive to the exact doping levels or to the thicknesses of the p and $p^+$ layers. However, the efficiency

is sensitive to $n^+$ thickness.[6] Our best cells so far have $n^+$ layers about 500 A thick. Although efficient cells have been fabricated with as-grown $n^+$ layers of this thickness, it is advantageous to grow a thicker $n^+$ layer and then to use an anodization and stripping process (with the front contact fingers and bars already in place) for controlled reduction of the thickness.[5] This process allows a variation in the as-grown $n^+$ thickness, as well as producing a larger separation between the front contacts and the junction, thus increasing the yield achieved in cell fabrication.

The cells are fabricated without any vacuum processing steps, utilizing an antireflection (AR) coating about 850 A thick prepared by anodic oxidation of the $n^+$ layer and electroplated Au or Sn front and back contacts. With Sn front contacts, anodization and stripping are readily accomplished, because a thin film of $SnO_2$ is formed on the top surface of these contacts during anodization, thus limiting electrolytic current leakage through the contacts.

Having succeeded in developing the highly efficient and versatile $n^+/p/p^+$ GaAs shallow-homojunction structure we are presently investigating processes to greatly reduce the weight of such cells without a significant reduction in cell efficiency. To retain high efficiency, we believe that the cells should utilize thin GaAs layers that are single crystalline.

## II. CLEFT PROCESS

### A. Material Growth

The CLEFT process permits the growth of thin single-crystal GaAs films by CVD on reusable GaAs substrates. Since many films can be obtained from one

substrate, this process should permit a marked reduction in material usage and cost; since single-crystal films are used, cell efficiencies should remain high; since the films are only a few microns thick, such cells can have very high power-to-weight ratios.

The CLEFT process is a peeled-film technique. The basic idea of peeled-film technology is to grow a thin single-crystal epilayer on a single-crystal mold, to separate the epilayer from the mold, and then to use the mold again (see Fig. 2). A chemical peeled-film technique has been reported[10] for GaAs. A thin single-crystal GaAs film was deposited by molecular beam epitaxy on a GaAlAs layer about 5 μm thick grown on a GaAs substrate. The GaAlAs intermediate layer was removed by selective etching with HF introduced through small openings at the edge of the substrate, and the GaAs film was then separated from the substrate (see Fig. 3). Conversion efficiency of 13.5% at AM1 has been achieved for GaAlAs/GaAs heteroface solar cells using GaAs films ~ 50 μm thick separated by this chemical technique.[10] Such a technique is inconvenient, however, even if the intermediate layer is relatively thick, since it is difficult to circulate an etchant through the small openings. The CLEFT process is an alternative that provides a practical way of separating epilayers from their substrates.

The key element of the CLEFT process is the use of lateral epitaxial growth performed in the $AsCl_3$-GaAs-$H_2$ reactor. Our experiments have shown that if a mask with appropriately spaced stripe openings is deposited on a (110) GaAs substrate, the epitaxial growth initiated on the GaAs surface exposed through the openings will be followed by lateral growth over the mask,

101430-R-03

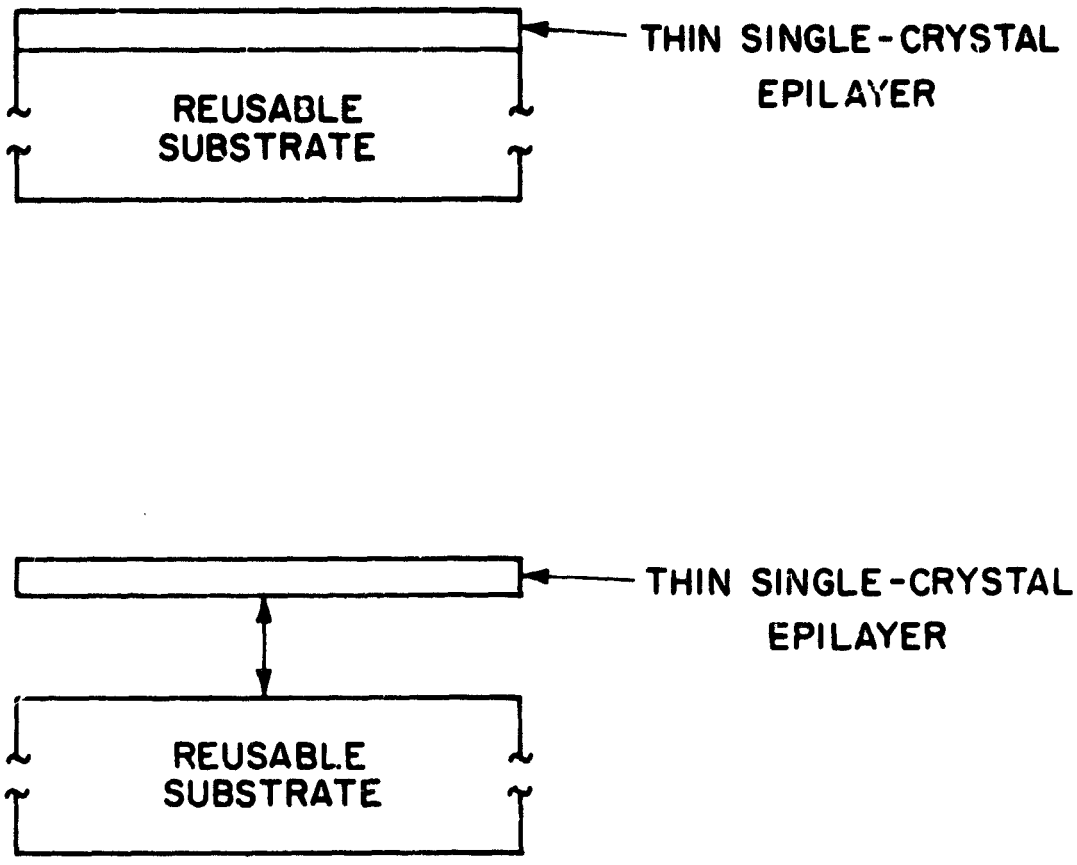


Fig. 2. Schematic diagram showing the peeled film technology.

101326-M

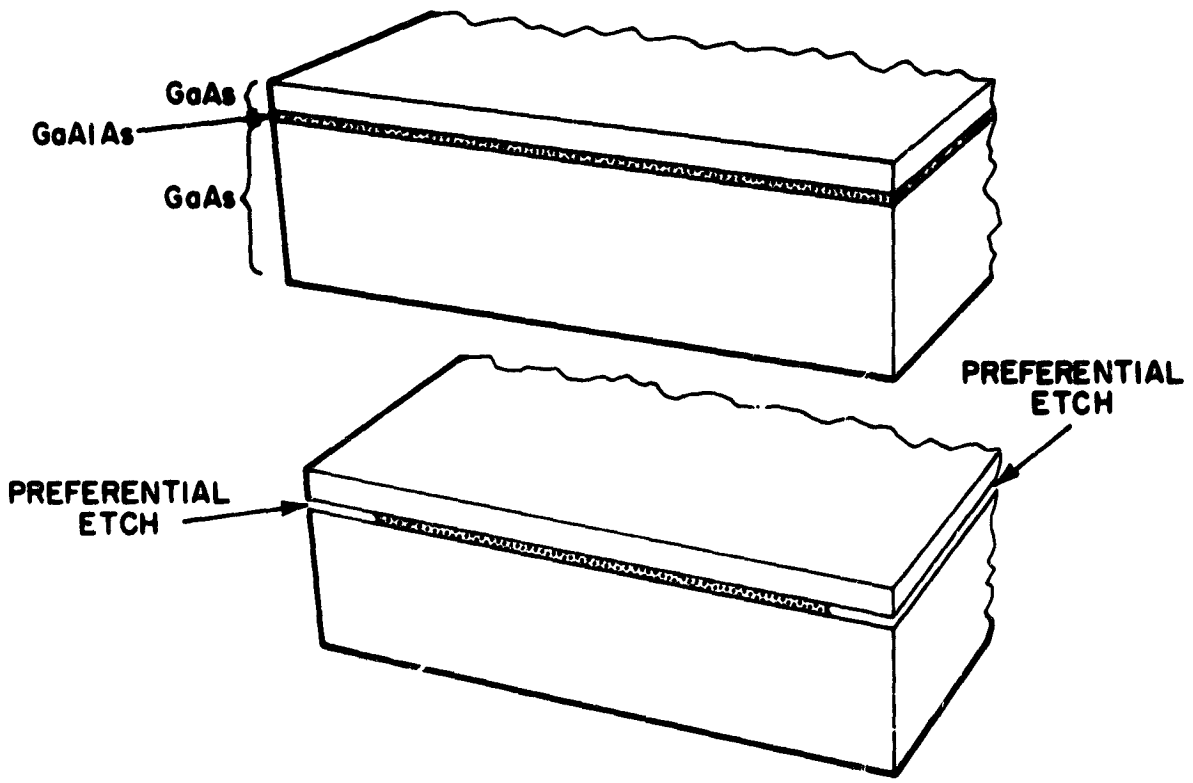


Fig. 3. Schematic diagram showing a chemical method for peeling a GaAs film.

eventually producing a continuous single-crystal film that can be grown to any desired thickness.[11] The upper surface of the film is then bonded to a secondary substrate of some other material. If there is poor adhesion between the mask material and the GaAs, the film will be strongly attached to the GaAs substrate only at the stripe openings. Since a weak plane has been created by the mask and because the (110) plane is the principal cleavage plane of GaAs, the film can be cleaved from the GaAs substrate without significant degradation of either (see Fig. 4). We have found that carbonized photoresist is a suitable mask material, since it has the necessary poor adhesion to GaAs and is chemically inert under the conditions that we employ for CVD growth. Other mask configurations have also been investigated, including $SiO_2$-coated carbonized photoresist masks which provide somewhat better surface morphology for GaAs CLEFT films.

The technique used for separating the GaAs film from the GaAs substrate is illustrated by the schematic diagram shown in Fig. 5. The upper surface of the film is bonded with epoxy to a glass secondary substrate. The GaAs and glass substrates are then bonded to glass plates that serve as cleaving supports. A wedge is inserted between the two glass plates and tapped gently, causing the GaAs film to be cleaved from the GaAs substrate but leaving it mounted on the glass substrate. Finally, the GaAs primary substrate is removed from its glass cleaving support plate, leaving it ready for another cycle of the process.

In using the mechanical cleavage scheme just described, it would be very desirable for the mask to remain with the substrate during cleavage, making it

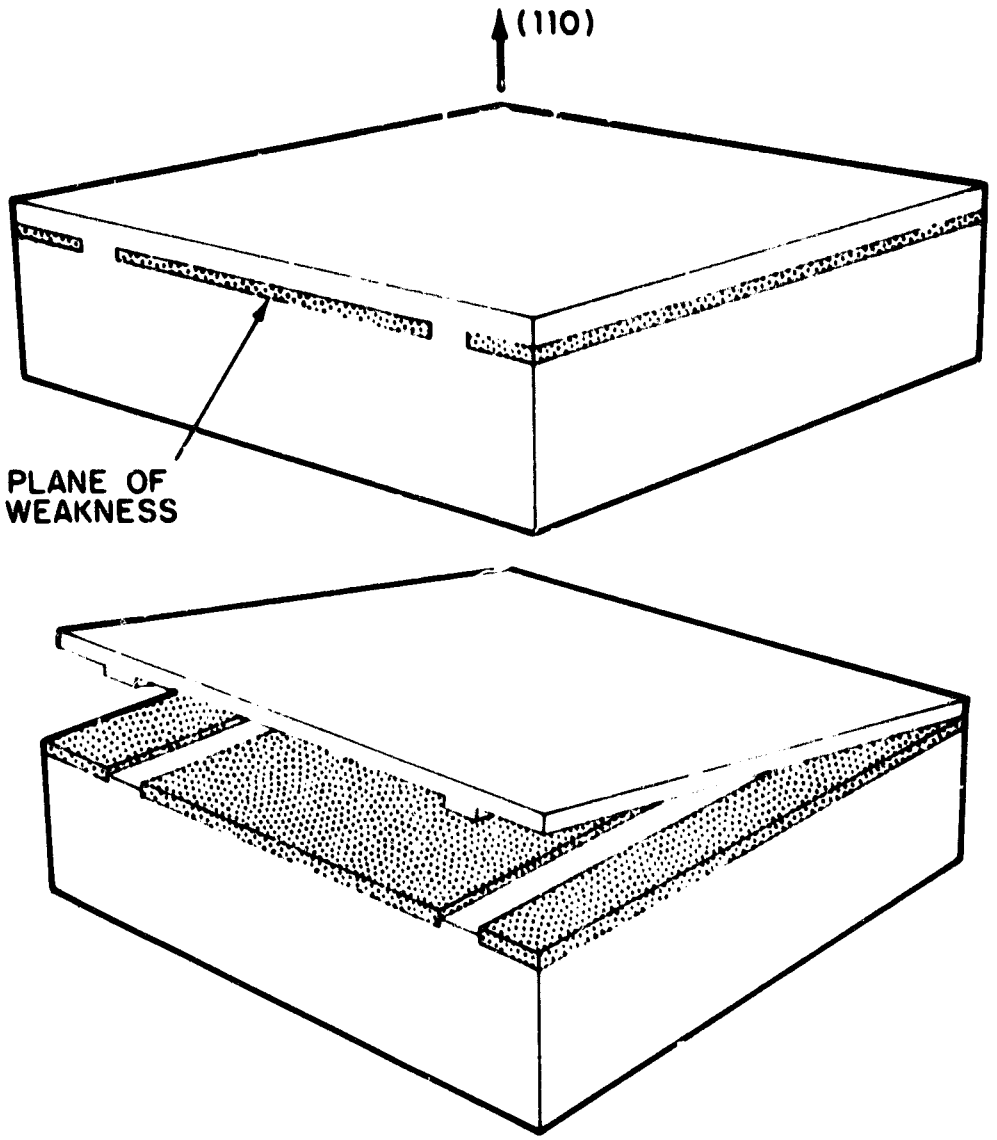


Fig. 4. Schematic diagram showing the CLEFT process of peeling a GaAs film.

100059-R-01

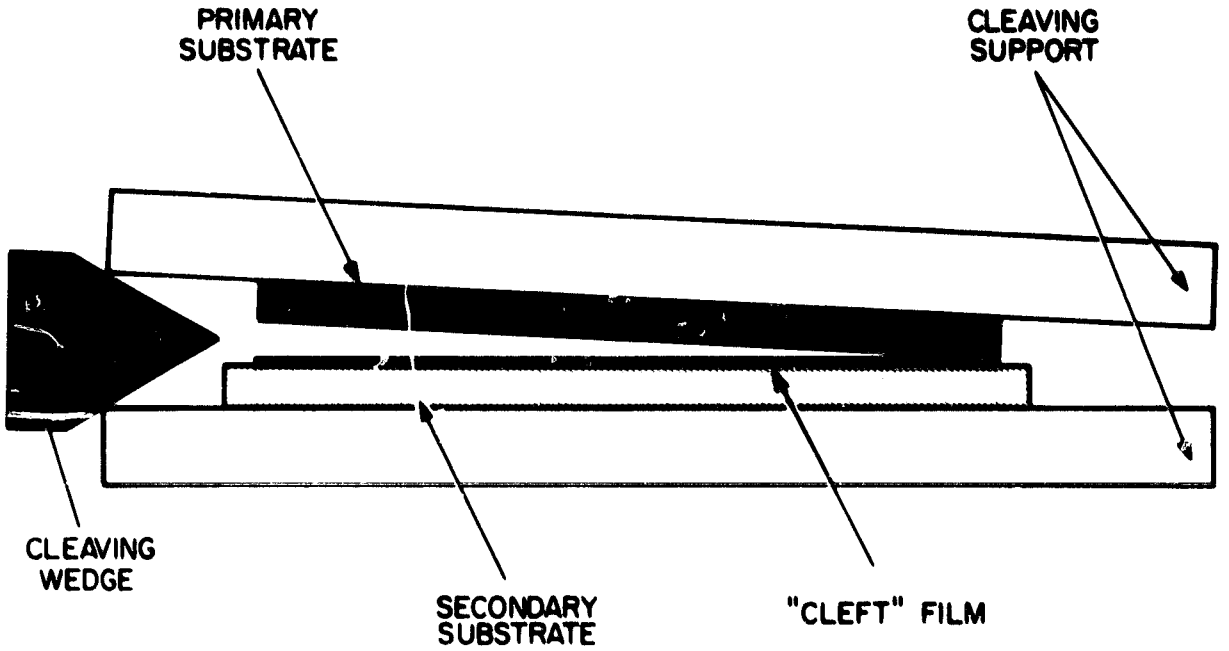


CLEFT - CLEAVAGE OF LATERAL EPITAXIAL FILMS FOR TRANSFER

Fig. 5. Cross-sectional view of a CLEFT epitaxial film being transferred from the GaAs substrate.

unnecessary to prepare a new mask after each successive film is transferred. This has been accomplished[12] with the modified mask structure shown in Fig. 6, which has a layer of evaporated silicon between the GaAs and the carbonized photoresist. The silicon adheres well to GaAs, and the carbon adheres to the silicon after heating to CVD VPE growth temperatures because of the formation of silicon carbide. Such a mask was used to make a CLEFT film, and the entire mask stayed with the substrate during cleavage. However, further experimentation is still needed on this particular type of mask configuration. As a demonstration that the CLEFT process can be used to prepare multiple GaAs films, we have carried out four CLEFT cycles with the same single-crystal GaAs substrate that were covered with carbonized photoresist mask. Four successive films of excellent quality were obtained, with thicknesses of 5, 10, 10, and 8 μm, respectively. The area of each film is about 4 $cm^2$. The films prepared and separated in this manner have been shown by Hall measurements to be comparable in quality to conventional single-crystal CVD layers.[11]

B. Solar Cell Fabrication

The following procedure has been used in making the CLEFT solar cells.[13] Photoresist is applied to the polished surface of a <110> GaAs wafer, thermally carbonized, and coated with a 1000 Å film of CVD $SiO_2$. Standard photolithographic techniques are then used to pattern the double masking layer with 2.5-μm-wide stripe openings on 50 μm centers. The $SiO_2$ inside the openings is removed by etching with buffered HF; the carbonized photoresist is removed by $He/O_2$ plasma etching. The resulting mask configuration is shown schematically in Fig. 7(a).

102713-N-01

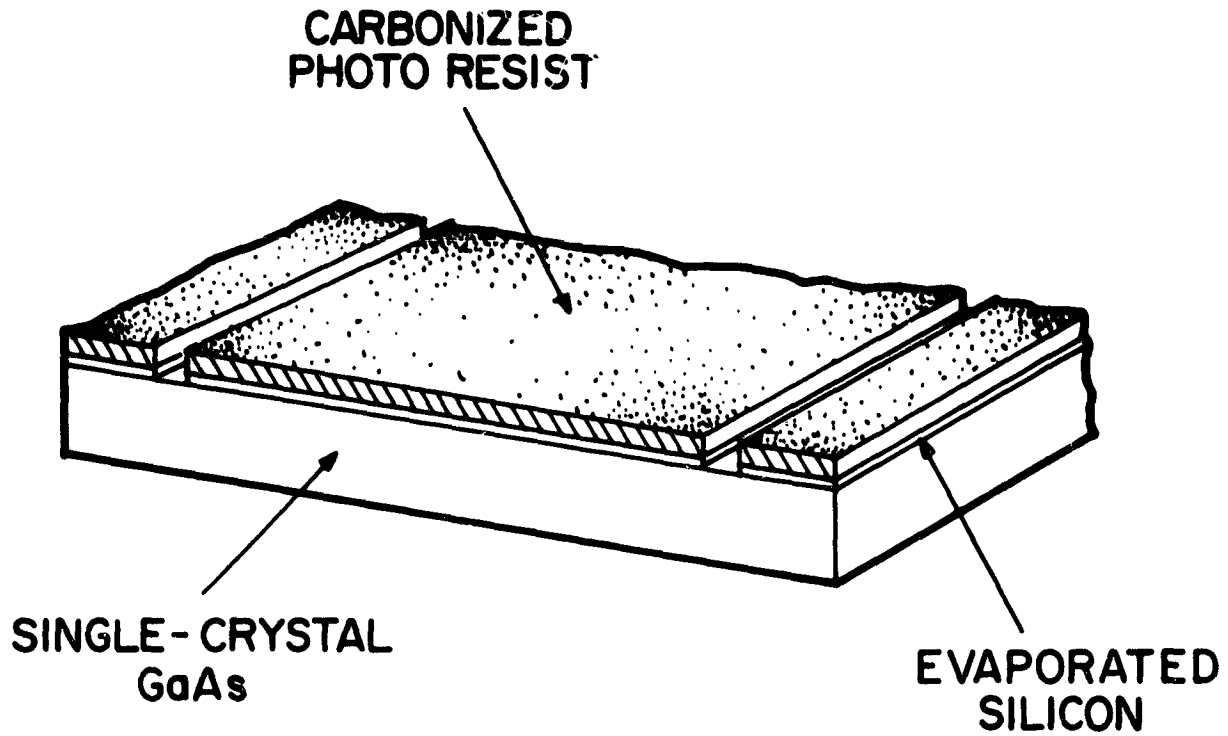


Fig. 6. A growth mask using silicon intermediate layer for improved adhesion to the substrate.

An epitaxial GaAs film is grown on the masked substrate at 700°C by the $AsCl_3$-GaAs-$H_2$ method described previously. Growth is seeded by the exposed GaAs substrate within the stripe openings. This initial growth is followed by lateral growth over the mask, which eventually produces a continuous single-crystal film that can then be grown to any desired thickness by vertical growth in the usual manner. Figure 7(b) shows a film at an intermediate stage after it has begun to grow over the mask but before it becomes continuous. Under the growth conditions used the ratio of lateral to vertical growth rates is about 10 to 1, so that the film becomes continuous when it is only about 3 μm thick, as shown in Fig. 7(c). After the film became continuous, a 5-μm-thick $p^+$ layer (1-3 x $10^{18}$ $cm^{-3}$), followed by a 2-μm-thick p layer (1 x $10^{17}$ $cm^{-3}$) and a 1500-Å-thick $n^+$ layer (5 x $10^{18}$ $cm^{-3}$) is grown in order to obtain the shallow-homojunction structure used for these solar cells. The acceptor dopant is Zn supplied by adding $(CH_3)_2Zn$ to the vapor stream, while the donor dopant is S provided by $H_2S$. The $n^+/p/p^+$ structure formed is shown schematically in Fig. 7(d).

The procedures used for contact metallization, $n^+$ layer thinning, and antireflection (AR) coating are quite similar to those employed for conventional GaAs shallow-homojunction cells.[4,5] Tin contact fingers are electroplated on the $n^+$ surface through openings in a photoresist mask, and the area of the cell is defined by a mesa etch. Anodic oxidation is then used to produce an AR coating and simultaneously to reduce the thickness of the $n^+$ layer, which results in an increase in carrier collection efficiency and therefore in cell conversion efficiency. The thickness of the $n^+$ layer is

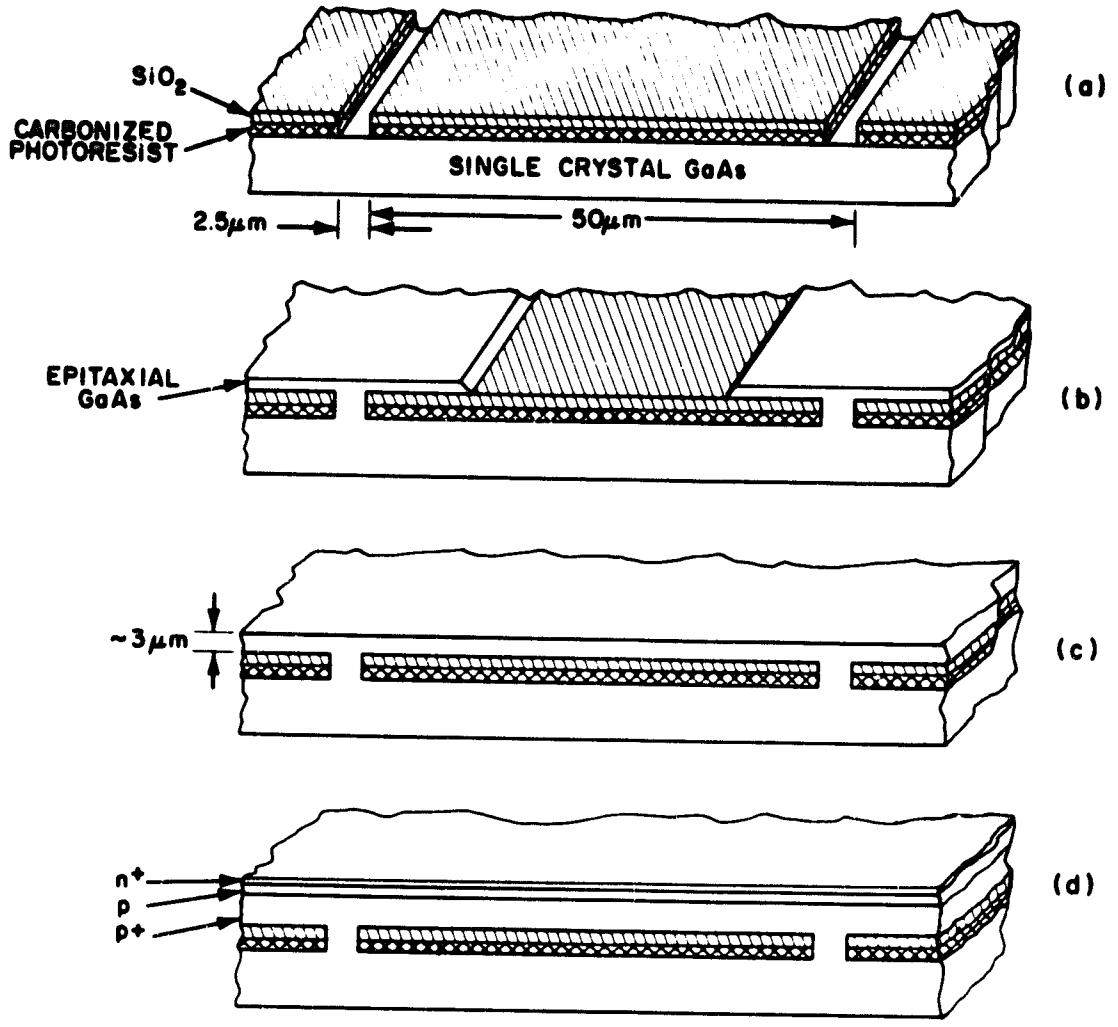


Fig. 7. Schematic diagram showing a GaAs film containing a $n^+/p/p^+$ shallow-homojunction formed by a lateral epitaxial overgrowth. In (a) the single-crystal substrate is shown before growth begins. In (b) and (c) the $p^+$ GaAs grows together laterally from the narrow stripe openings to form a single-crystal film. Growth is continued in (d) to form the homojunction.

reduced from its initial value of about 1500 A to about 500 A by alternating anodic oxidation and etching steps.[5] The last of these steps is an anodization that forms an oxide layer about 850 A thick to serve as the AR coating.

The technique used for separating the metallized and anodized GaAs film from the GaAs substrate is essentially the same as in the initial CLEFT experiments.[11] The upper surface of the film is bonded with transparent epoxy to the uncoated side of a $MgF_2$-coated glass substrate that serves as the cell cover glass. The GaAs and glass substrates are then bonded with wax to glass plates about 5 mm thick that serve as cleaving supports. A metal wedge is inserted between the two glass plates and gently tapped. Because the photoresist-$SiO_2$ mask has poor adhesion to GaAs and the (110) plane is the principal cleavage plane of GaAs, the GaAs film is cleaved from the GaAs substrate but remains mounted on the glass substrate. The GaAs substrate can then be prepared for another cycle of the CLEFT process.

To complete solar cell fabrication, the cell structure is removed from the glass cleaving support plate, gold is electroplated on the cleaved surface of the GaAs film to form the back contact, and an opening is etched in the film to expose the front contact pad. Figure 8 is a schematic diagram of a portion of a completed cell in cross section. The GaAs film is completely encapsulated by epoxy and glass on the front surface and by gold on the back surface.

Three CLEFT cells have been fabricated from GaAs films that were grown on different GaAs substrates in separate CVD runs. Table I lists the area, cover glass thickness, open-circuit voltage, closed-circuit current density, fill

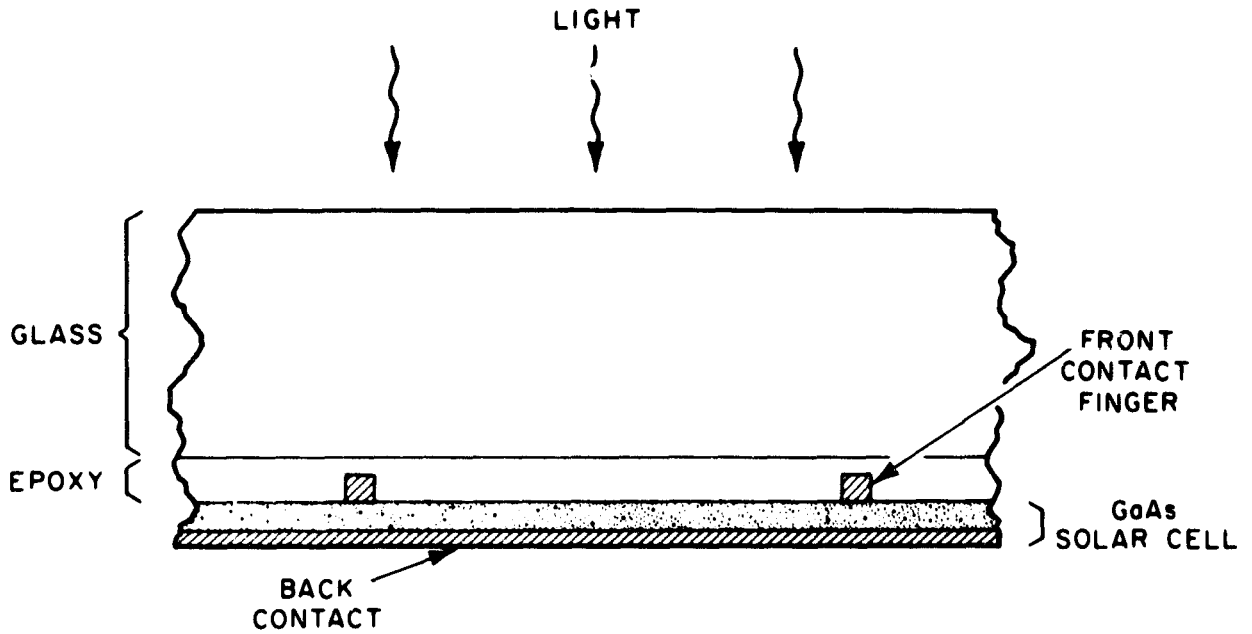


Fig. 8. Cross-sectional view of completed CLEFT cell, in which the glass substrate serves as the protective cover glass.

TABLE I

PARAMETERS OF CLEFT SOLAR CELLS

| | Area ($cm^2$) | Cover glass thickness ($\mu m$) | Open-circuit voltage (V) | Short circuit current density ($mA/cm^2$) | Fill factor | Conversion efficiency (AM1) % |
|---|---|---|---|---|---|---|
| Cell 1 | 0.36 | 500 | 0.92 | 22 | 0.73 | 15 |
| Cell 2 | 0.51 | 500 | 0.94 | 23 | 0.79 | 17 |
| Cell 3 | 0.51 | 100 | 0.89 | 23 | 0.74 | 15 |

factor and AM1 conversion efficiency of each cell. For power conversion efficiency measurements a high-pressure Xe lamp with a water filter was used as a simulated AM1 source, calibrated with a NASA-measured GaAs reference solar cell. The efficiencies of cells 1, 2 and 3 are 15, 17, and 15%, respectively. The cover glass of cell 3 is a special lightweight device made by using a glass substrate only 100 μm thick and limiting the glass and GaAs film to an area only slightly larger than the cell area. Including the weight of the cover glass, cell 3 weighs only 0.023 g, giving rise to a power to weight ratio of 340 W/kg at AM1 and 380 W/kg at AM0.

The external quantum efficiency of the 17% cell is plotted as a function of wavelength in Fig. 9. This quantum efficiency is somewhat less than that of our best conventional shallow-homojunction cells, because of reflection at the GaAs-epoxy interface. The anodic oxide used for AR coating is optimum for the air-GaAs interface and therefore not optimum for the epoxy-GaAs interface. The reflectivity could be reduced by substituting $Si_3N_4$ for the anodic oxide. In addition, the solar transmission of the CLEFT cells is reduced by a few percent due to reflection at the glass-air interface, even though the cover glass is AR coated with $MgF_2$.

The CLEFT process allows a drastic reduction in the usage of GaAs--an essential requirement for cells made of semiconductors that are much less plentiful than Si. The reduction in material usage does not result in significant degradation in the high efficiency of GaAs cells, which is their major advantage over Si cells. Cell modules having high conversion efficiency will provide a substantial economic and weight advantage over modules of lower

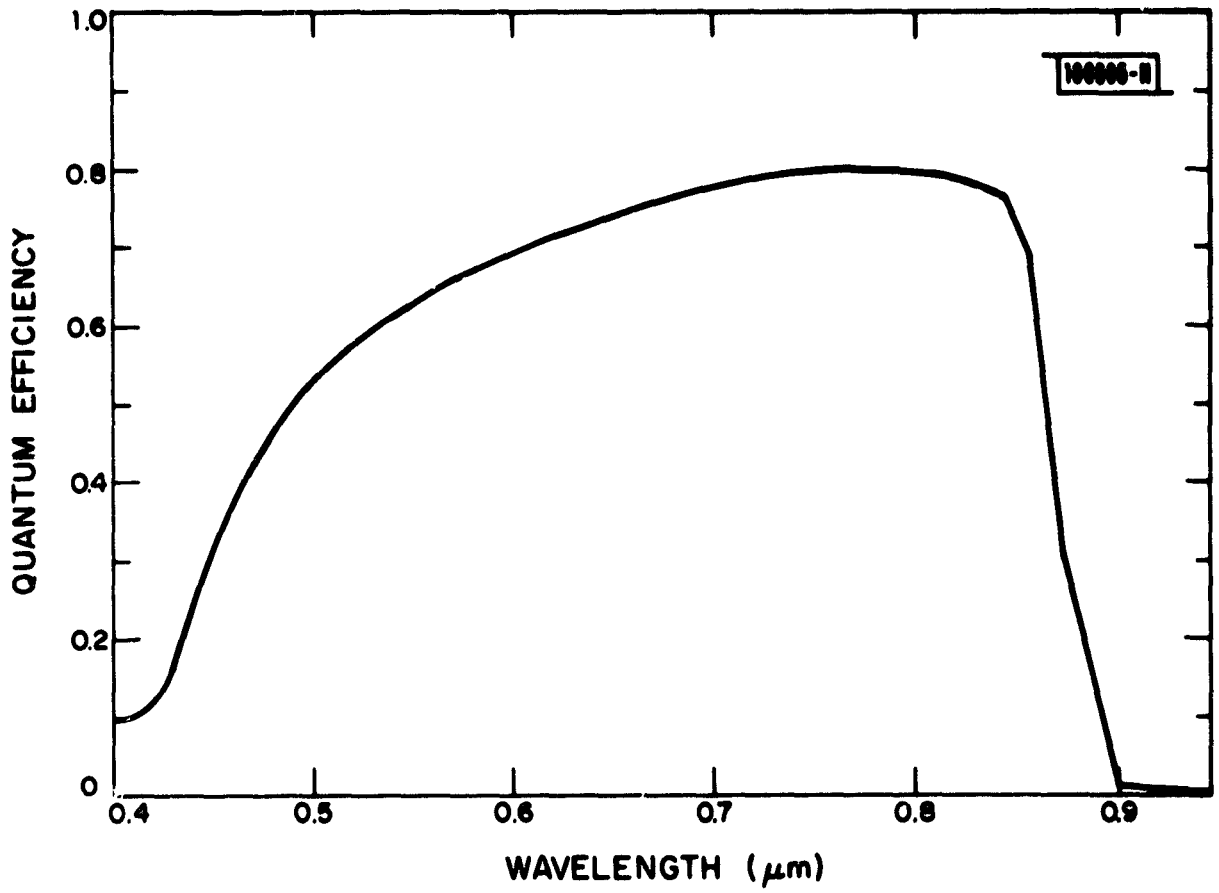


Fig. 9. External quantum efficiency as a function of wavelength for the CLEFT cell with conversion efficiency of 17% (AM1).

efficiencies. It is expected that CLEFT cells, when fully developed, will achieve conversion efficiencies as high as 20% with GaAs layers only 5 μm thick. If this goal can be achieved, the cost of GaAs material will no longer be the major obstacle for this material system. Furthermore, there should be enough Ga available for large-scale deployment of GaAs cells.[14]

Figure 10 lists the basic material costs[15] for Si and GaAs cells, estimated from the current prices of electronic grade GaAs and Si raw material. For GaAs modules made from 5-μm-thick, 18% efficient cells (AM1) the GaAs material cost is about $\$12/m^2$, or $\$0.07/W_p$. For Si modules made from 125-μm-thick cells, the Si material cost is $\$18/m^2$ or $\$0.13/W_p$. While the price of raw polysilicon may come down from the current price, especially if material of poorer quality than electronic grade can be used, the price of GaAs raw material may also be reduced for the same reason. In addition, the actual material costs in modules are dependent on the material processing techniques used. In any case, Fig. 10 indicates that the material costs of GaAs cells made by the CLEFT process should present no obstacle to their use in flat-plate modules.

Concentrator cells made of GaAs have a basic advantage over Si cells because of their higher conversion efficiencies. However, to avoid a significant reduction in concentrator cell efficiency, it is necessary to maintain low operating temperatures. Since the thermal conductivity of GaAs is only about 1/3 that of Si, cooling of bulk GaAs cells has been a problem. This difficulty should not arise for CLEFT cells, which are so thin that

BASIC MATERIAL COST

| MATERIAL | CURRENT 1981 PRICE* ($/kg) | THICKNESS (μm) | WEIGHT ($g/m^2$) | MODULE % (AM1) | $/$m^2$ | $/$W_p$ |
|---|---|---|---|---|---|---|
| Si | 60 | 125 (5 mil) | 290 | 14 | 18 | 0.13 |
| GaAs | 450 | 5 | 26 | 18 | 12 | 0.07 |

*ELECTRONIC GRADE, POLYCRYSTAL

Fig. 10. Basic materials cost of Si and GaAs solar cells.

excellent heat-sinking can be obtained by mounting them directly on cooling blocks.

Finally, CLEFT cells suggest a promising alternative structure for high-efficiency tandem cells. Instead of the commonly conceived monolithic structure, CLEFT cells of different materials can be stacked (Fig. 11) on top of a bulk cell. For a three-cell structure, for instance, a CLEFT GaAlAs cell and a CLEFT GaAs cell could be placed on top of a Ge cell. The resulting tandem cell should have high conversion efficiency. The three cells could be connected in series or parallel, depending on whether the bonding material is conducting or insulating. For tandem cells of the proposed structure to be practicable, the upper cells must have very thin layers in order to reduce parasitic optical absorption. The CLEFT cells satisfy this requirement very well.

As noted earlier, solar cells used in space must be radiation resistant, highly efficient, and light in weight. Our $n^+/p/p^+$ shallow-homojunction structure has already satisfied the efficiency and radiation resistance requirements. The CLEFT cells now offer the possibility of very light weight solar cell panels.

Because the density of GaAs is about a factor of two larger than that of Si, there is a common misconception that GaAs solar cells must be heavier than Si cells. However, because of the much stronger optical absorption of GaAs, GaAs cells actually have the potential to achieve specific power (power/weight) several times larger than that of Si cells. As an illustration, a 5-μm-thick 18% (AMO) GaAs solar cell will have a specific

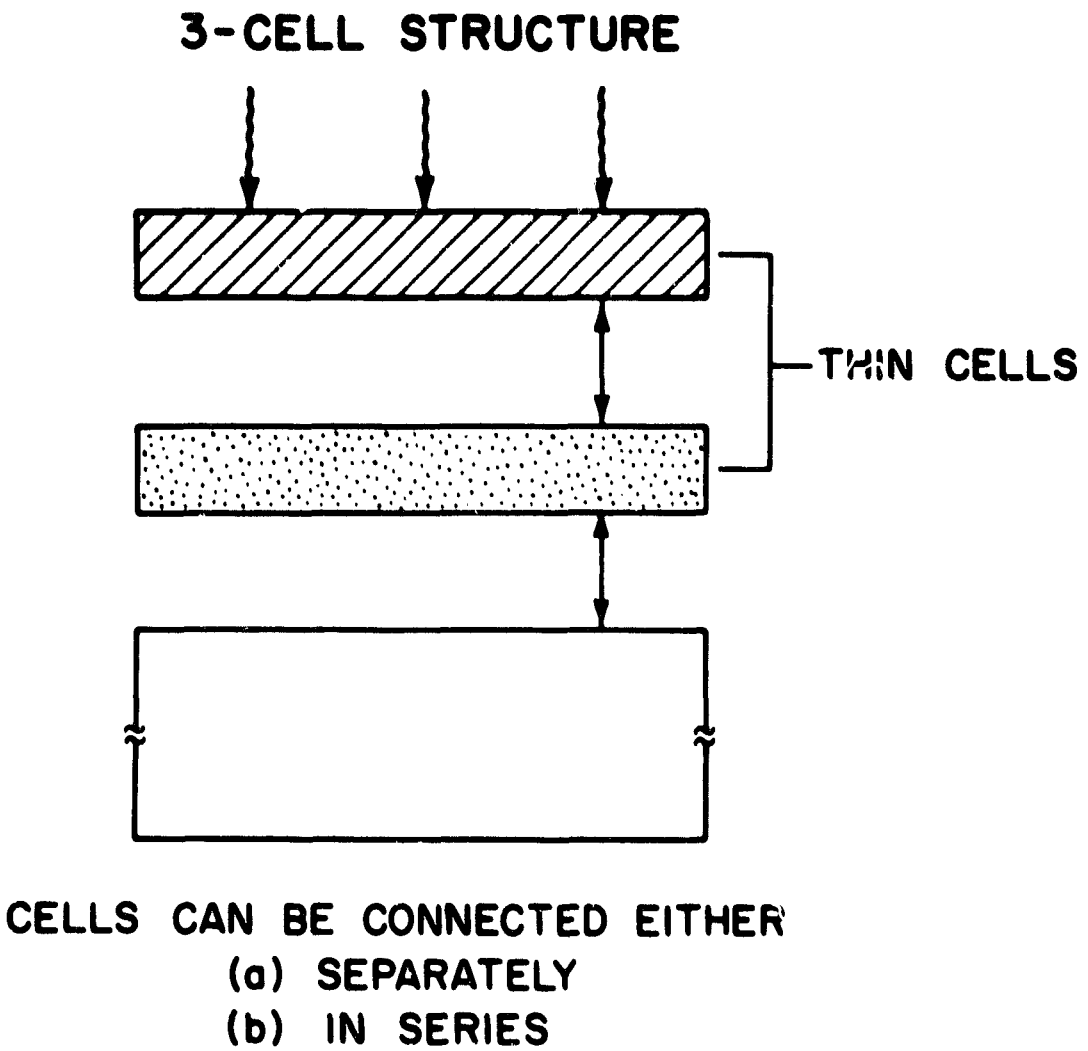


Fig. 11. A three-cell tandem structure illustrating a proposed application of CLEFT solar cells.

power of about 9.3 kW per kilogram of GaAs. The specific power of the complete cell will be reduced by the weight of contacts and bonding material, which is not very significant, and also by the weight of the cover glass, which is indeed very substantial. Even for a 100-μm-thick cover glass that we have used, the glass will be many times heavier than the GaAs. Therefore, for ultralight cells even thinner glass must be used. A lower limit on the thickness is set by the requirement that the cover glass be thick enough to prevent cell degradation under proton bombardment. However, by using high-efficiency CLEFT cells with proper lightweight packaging it should be possible to produce panels with specific power over several kW/kg.

C. Potential Production Schemes

By means of the CLEFT process thin semiconductor sheets and grown p-n junctions can be prepared in a single operation. In addition, the reuse of the GaAs substrates will greatly reduce the material and processing costs of GaAs wafers. Overall, as illustrated in Fig. 12, the CLEFT process makes it possible to eliminate many steps used in conventional solar cell processing, with substantial potential savings.

The major development still required is the scale-up of the CLEFT process to much larger areas. A possible production concept[15] is presented in Fig. 13, which shows a proposed master-panel structure for CLEFT growth. This panel is constructed by bonding a ceramic sheet to an assembly of GaAs tiles that are composed of GaAs layers pre-grown on single-crystal Ge wafers. The Ge wafers are used because crystals of Ge, which has a good lattice match to GaAs, can currently be grown with much larger dimension than GaAs crystals. The master

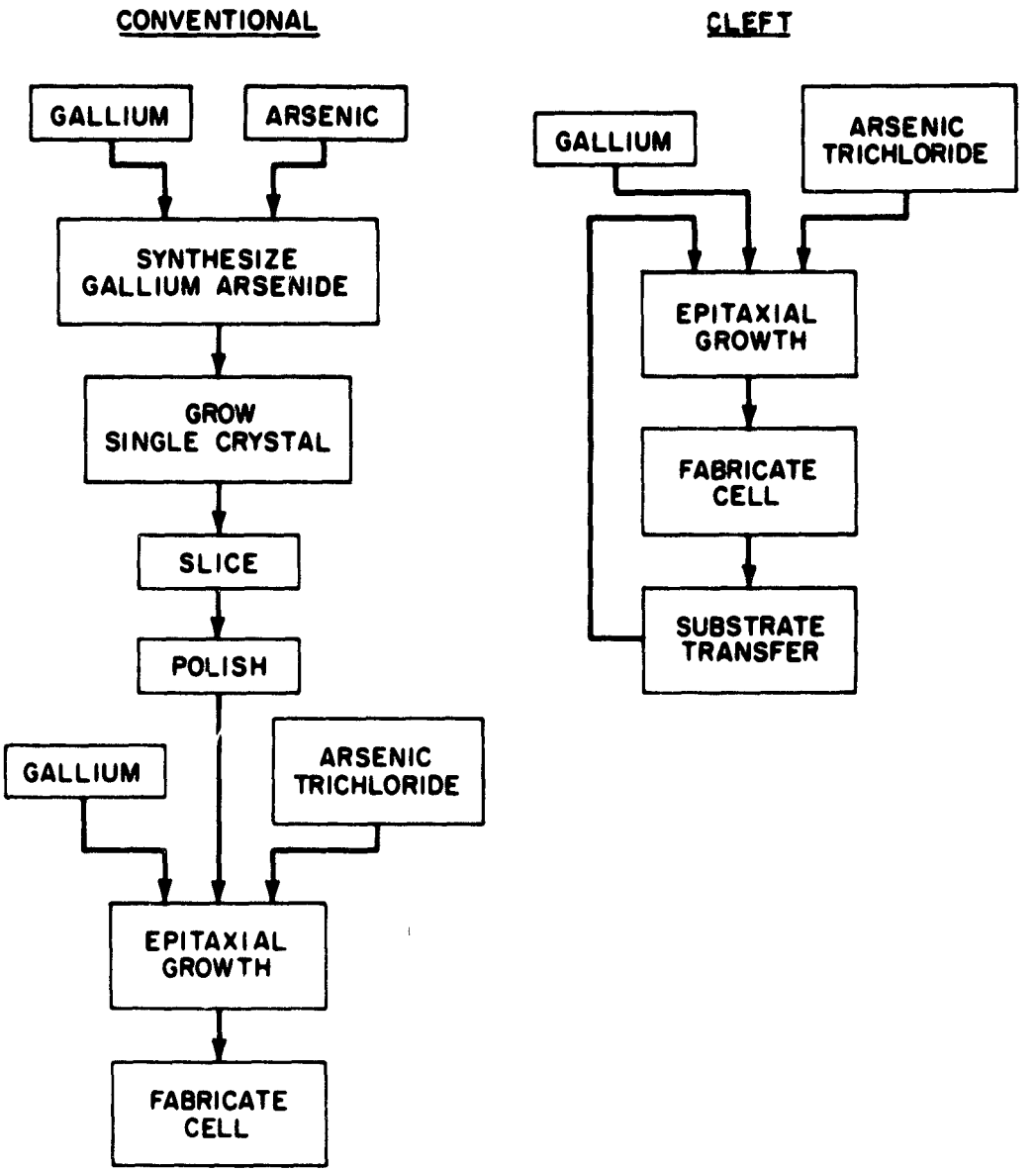


Fig. 12. Flow charts illustrating the processing steps required for conventional GaAs cells for CLEFT GaAs cells.

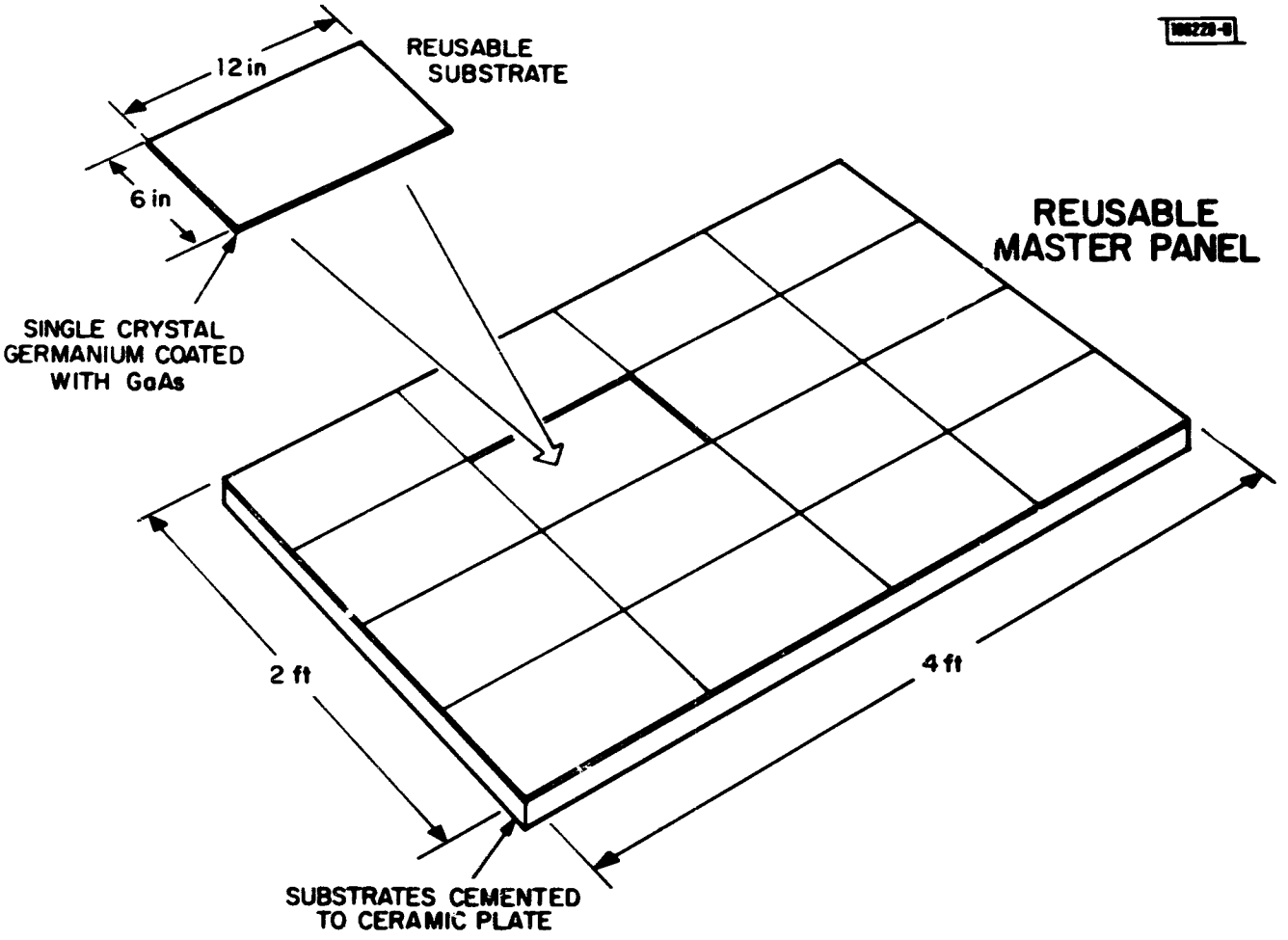


Fig. 13. Proposed GaAs reusable master panel composed of GaAs-coated Ge substrated bonded to a ceramic plate.

panel shown has dimensions of 2 feet by 4 feet. While such a large size may be too ambitious initially, smaller panels may well be economical. The master panels would be employed as the reusable GaAs substrates that we have demonstrated in the laboratory. These panels are placed in large CVD reactors for lateral overgrowth and formation of the p-n junction. After growth, front contacts and AR coatings are formed on the front surface. The whole panel is bonded to a large glass sheet, and all the GaAs cells, each from one GaAs tile, are simultaneously transferred to the cover glass. The back contacts, interconnects and back encapsulation are formed in the final operations (Fig. 14). The whole process not only saves many steps in cell fabrication but will also eliminate several encapsulation and packaging steps. There are, however, many difficult problems to be solved in implementing this scheme, including achieving uniform CVD growth over large areas and developing bonding, separation, and interconnect techniques.

In summary our development of $n^+/p/p^+$ shallow-homojunction GaAs solar cells has demonstrated the feasibility of preparing high-efficiency, ultrathin GaAs cells. Both the material growth and device fabrication techniques should be compatible with mass production of these cells, and the cost and availability of semiconductor material no longer constitute major obstacles. Such cells have a bright future in both terrestrial and space applications.

## III. DESIGN AND CONSTRUCTION OF THE ORGANOMETALLIC CHEMICAL VAPOR DEPOSITION (OMCVD) SYSTEM

A new III-V CVD system using organometallic sources was designed and constructed. The system will be used to produce GaAs shallow-homojunction

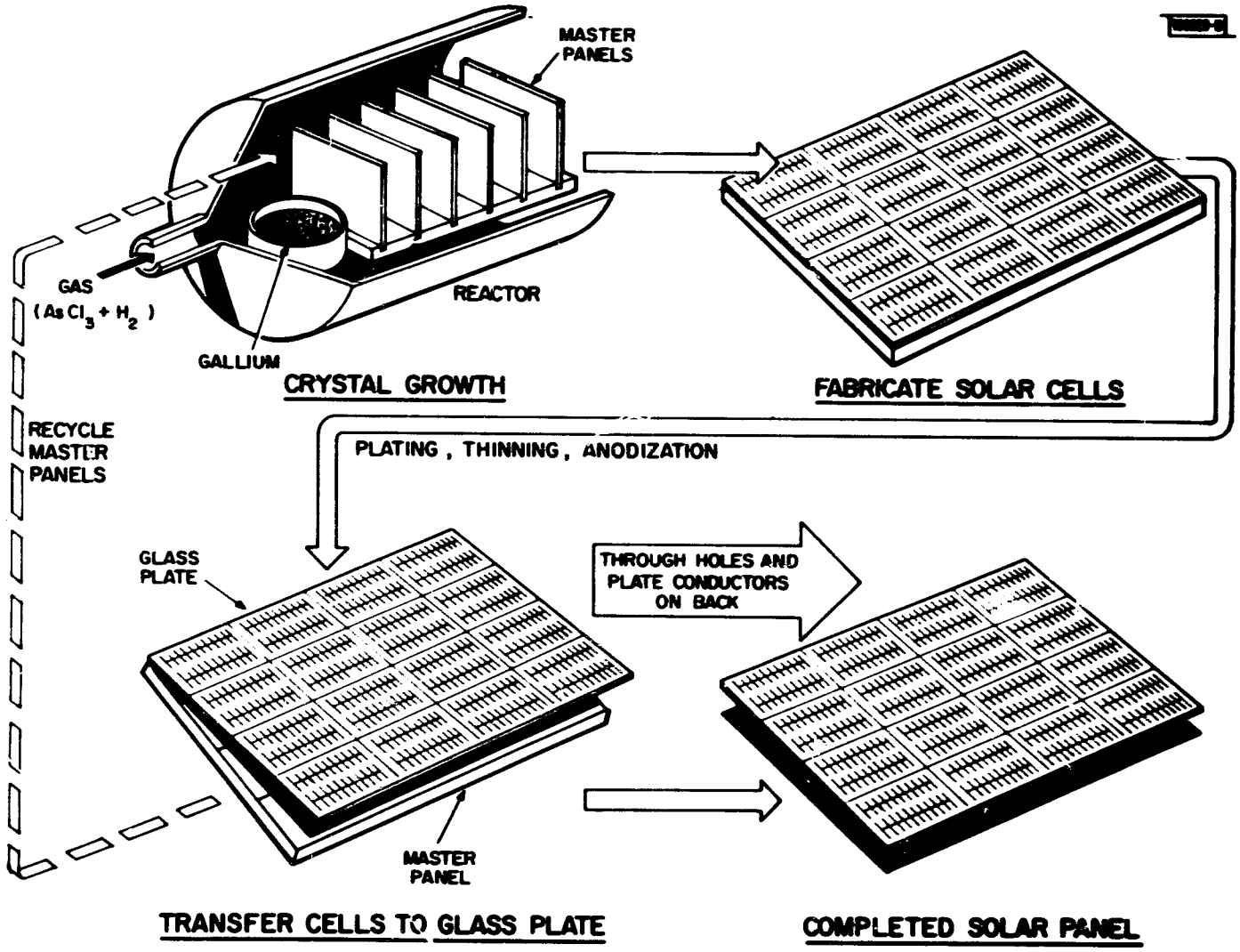


Fig. 14. Proposed production scheme for large-area CLEFT GaAs solar cell modules using reusable master panels.

solar cell structures for fabrication of high efficiency solar cells; to investigate GaAs and III-V ternary overgrowth for CLEFT cells; and to produce monolithic tandem cell structures. To satisfy these goals we have designed and built a growth system that is capable of utilizing the flexibility inherent to the OMCVD process. The new system is expected to produce GaAs layers shortly. Details of the OMCVD system are presented in the three following sections: the gas manifold, the control system, and the reactor.

A. Manifold Design

The gas manifold is designed to take full advantage of the flexibility of the OMCVD process. A total of eight source lines can be injected into one of the two manifolds which are mixed prior to entry into the reactor tube. A schematic is shown in Fig. 15. Flow parameters of the $H_2$ carrier gas and the source gases are controlled by pneumatic valves and electronic mass flow controllers, which are discussed in the following paragraph on construction. The OM manifold, on the right hand side of Fig. 15, is capable of independently handling up to three organometallic source bubblers. The amount of OM source material injected into the reactor is determined by the temperature of the liquid in the bubbler and the flow of hydrogen through it. The main manifold has inject lines for two group five source mixtures (5% $AsH_3$ in $H_2$ and 10% $PH_3$ in $H_2$), an HCl mixture (1% HCl in $H_2$), and two dopant lines. The design for the dopant lines was taken from our existing $AsCl_3$-GaAs-$H_2$ CVD system and can utilize five dopant mixtures in diluent systems allowing doping over three decades for each mixture. Initial transients in all inject lines are minimized by setting source flow conditions while the line is being vented

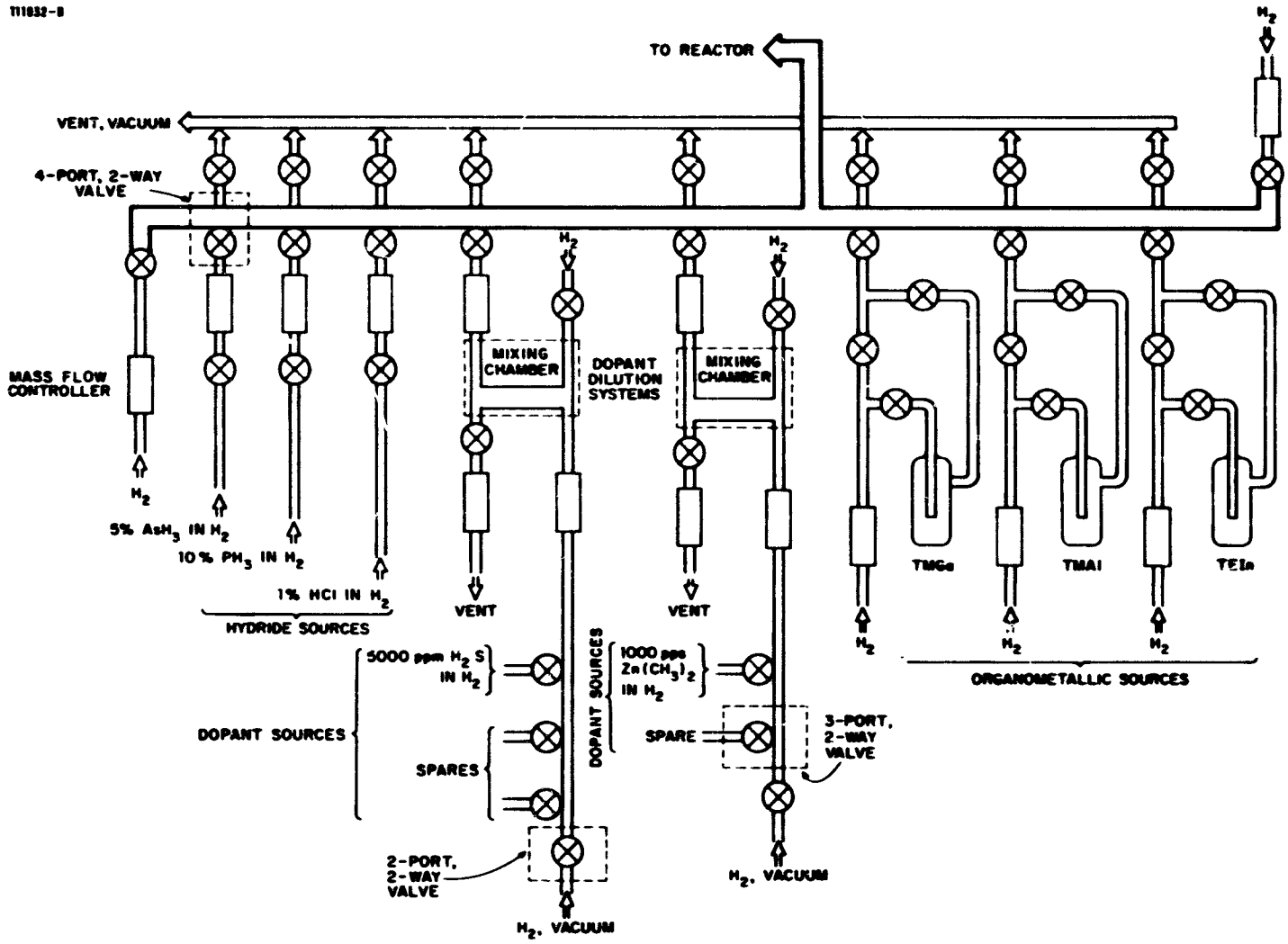


Fig. 15. Schematic diagram of the gas manifold of the OM CVD system.

to the exhaust. When a gas is to be introduced into the reactor, its inject valve is opened and its vent valve is closed, diverting the established flow into one of the manifolds. Each manifold has its own steady flow of hydrogen which quickly carries the injected gases to the reactor. This design should provide the system with excellent control over sharpness of both dopant and compositional profiles.

We applied much of our experience with our $AsCl_3$-GaAs-$H_2$ CVD system to the equipment and materials used in the constructuion of the OMCVD gas manifold. Tubing and fittings are stainless steel, welded wherever possible. Valves and mass flow controllers have Cajon VCR® fittings with a stainless steel gasket. The VCR® couplings are vacuum tight and allow for individual component removal. The valves are pneumatic-operated stainless steel bellows valves in one of three configurations: two-port/two-way for on-off operation, three-port/two-way for manifolding the dopant tanks, and four-port/two-way for the eight inject lines to allow for venting the source lines. The electronic mass flow controllers are Tylan's model FC-260 calibrated for various flow ranges of hydrogen. The hydrogen carrier gas is supplied from a Milton-Roy Hydrogen Purifier. In addition, the manifold may be evacuated selectively or purged with helium.

The physical layout of the manifold is compact, occupying a panel area of 4' x 3'. On the other side of this panel is the reactor, allowing the inject line to the reactor to be less than two feet in length. The manifold is contained within a cabinet vented to exhaust, which also contains the source

tanks. Most of the lines from the source tanks to the manifold are also less than two feet in length.

B. Control

The control functions are located directly above the cabinets that house the manifold and reactor. Figure 16 shows a block diagram of the components of the control system and the pathways that information is transmitted. The OMCVD system can be controlled either manually or by computer, determined by a control panel switch. The primary function of the digital and analog control boards is to select from which source the system controlling signals originate. The digital signals are used for driving relays as well as indicator lights on the control panel and input signals to the computer, allowing simultaneous monitoring of the valve positions by the computer and front panel. The analog signals are directed to the mass flow contollers, whose flow meter outputs are then also monitored by both the computer and front panel. In this manner the system status can be observed in each of two ways independently of system control.

The digital control board serves several additional functions as well. Because of the large number of valves in the manifold, many valves are represented on the control panel in functional groups, with up to three valves being controlled on the digital control board by only one switch. There are also three safety features contained on the board that are intended to prevent system contamination (or catastrophe). The first is a "watchdog" function, which monotors the computer and disengages computer control at any evidence of malfunction. The second safety feature is a protect function, enabled from

111981-A

# OM CVD CONTROL SCHEMATIC

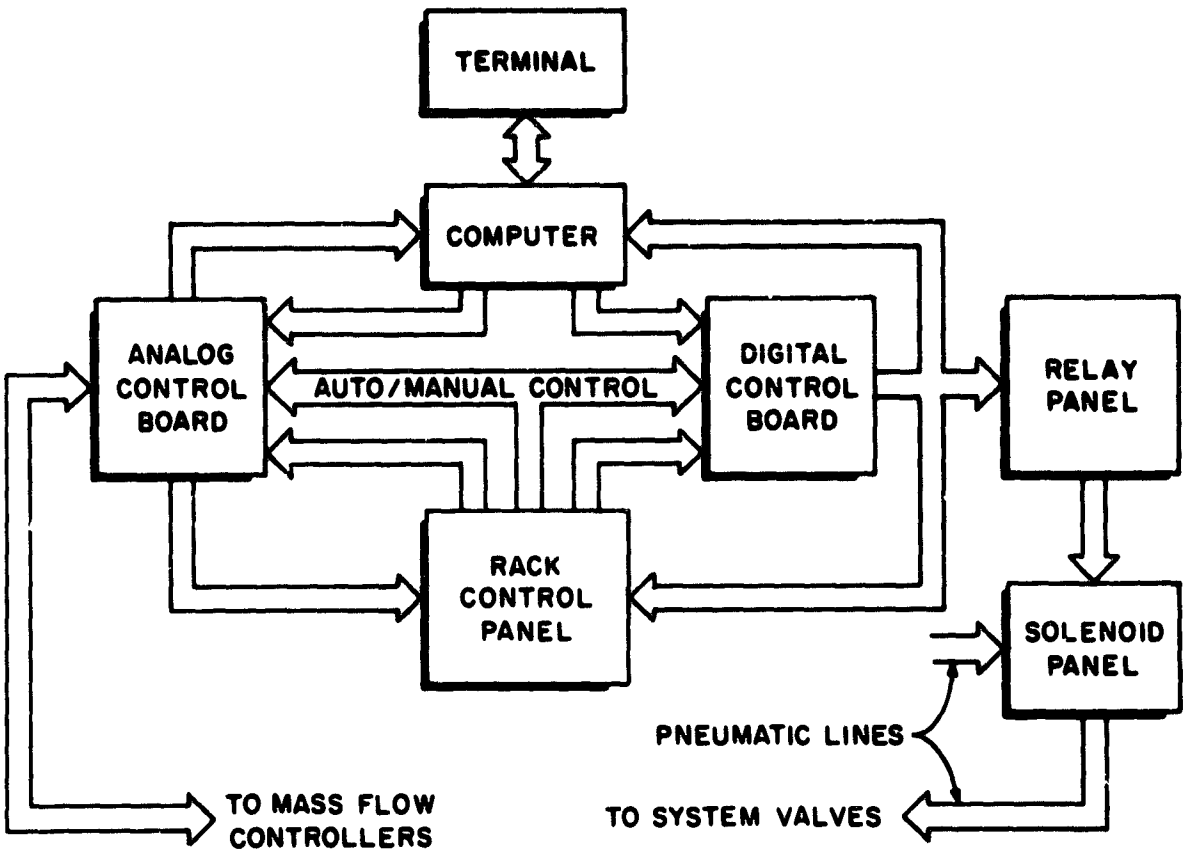


Fig. 16. Block diagram of the control system for the OM CVD system.

the control panel, which prevents any combination of valve position that would have an adverse effect on system operation. The protect mode would prevent operator or computer error from cross-contaminating the system. Finally, each output signal from the digital control board passes through a board-mounted switch which can disable any output. Thus, a valve that leads to a line that is not in use (such as an extra doping or OM source line) can be prevented from being activated.

The control system has been assembled and tested. The computer, an Analog Devices MACSYM 2, will be interfaced to the system shortly after the inital series of growth runs.

C. Reactor

The reactor is mounted horizontally with an inlet from the manifold, an outlet to the exhaust line, and a sample loading port. The reactor tube is approximately three feet long with an internal diameter of 65 mm, and is constructed completely of quartz to allow for ease of cleaning. The horizontal configuration was chosen to establish laminar flow conditions in the reactor above the substrate. Uniformity of growth will be controlled in part by adjusting the angle between the substrate surface, and the reactor axis. The inlet line is flexible to allow for the reactor to be mounted at a range of angles to the substrate surface, which will be maintained at horizontal plane. The exhaust line, connected to the reactor with an O-ring ball and socket joint, leads to a water bubbler and charcoal filter before being vented into the exhaust line.

## IV. FABRICATION OF 2cm X 2cm GaAs CELLS.

We have previously succeeded in fabricating 2cm x 2cm GaAs solar cells with conversion efficiency as high as 15.6% at AM0 (Reference 16). A practical conversion efficiency for such shallow-homojunction cells will be at least 17% AM0, and perhaps as high as 18% AM0. During this past year, we have been studying fabrication techniques to accomplish this goal. There are three major areas that have been closely examined.

### A. Growth Over Large Areas

Since the conversion efficiency of a shallow-homojunction cell is sensitive to the thickness of $n^+$ layer, the $n^+$ layer must be uniform over the cell area. In addition, the surface morphology of the grown layers must be smooth, and free of hillocks over the 2cm x 2cm area. Furthermore, for high efficiency cells, the $n^+/p/p^+$ structures with their respective doping levels and thicknesses must be close to optimum. According to our experience and our computer simulation, our $n^+/p/p^+$ have been close to optimum, and it is really a matter of growing high-quality uniform layers with excellent surface morphology. Considerable efforts have to be spent to obtain these layers, and we have recently succeeded in obtaining these layers repeatedly, through careful surface cleaning and preparation.

### B. Grid Design

Our basic fabrication techniques have been described in detail in our previous report.[16] There is, however, a change in the front contact grid design. The original contact grid pattern (see Fig. 17) for the 2cm x 2cm cell had a number of disadvantages. Both the placement of the central "bow

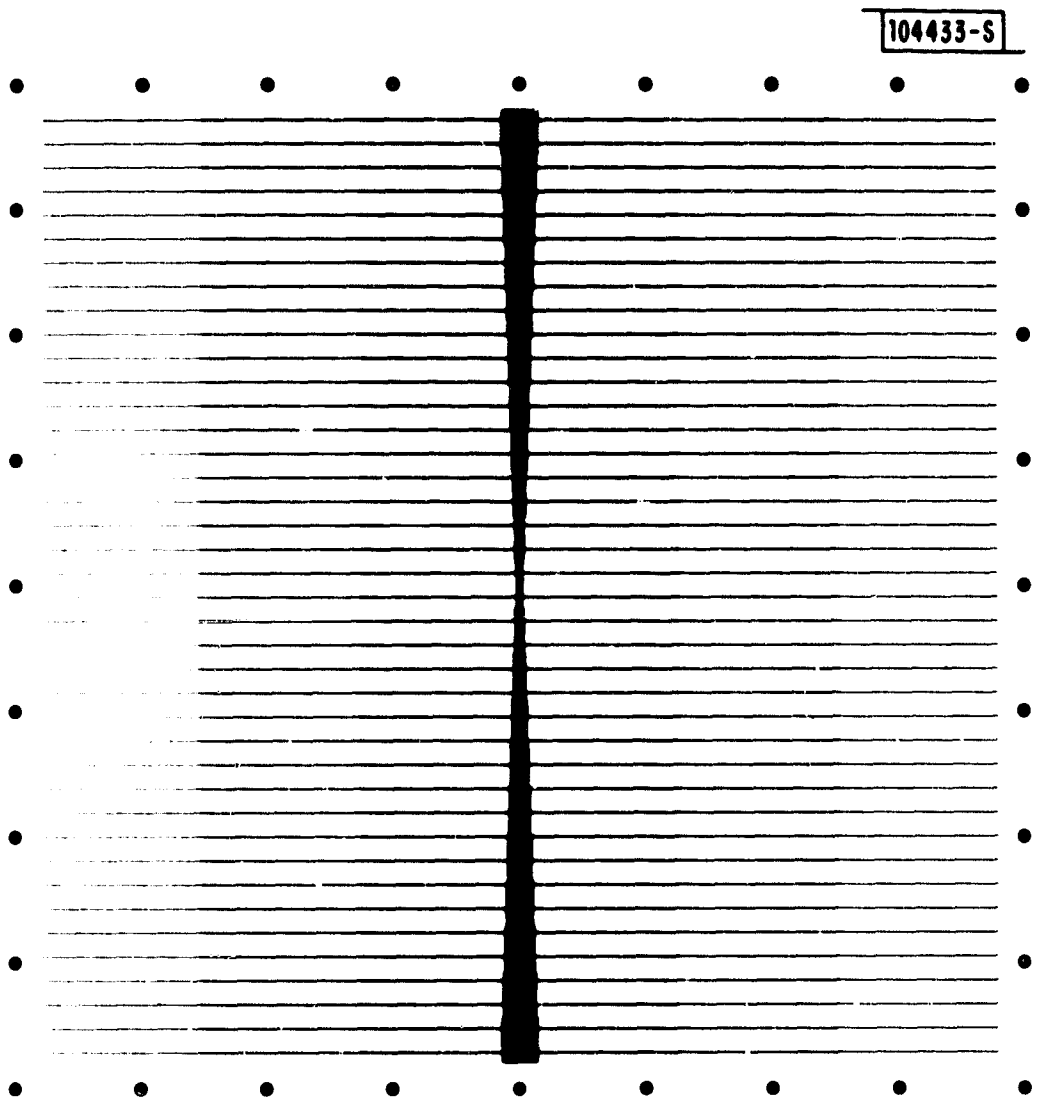


Fig. 17. Schematic diagram of the original front contact mask. Small circular dots at perimeter of mask are contact dots for small test mesa cells.

tie" busbar and the geometry of the fingers themselves increased the obscuration of the active area. In addition, the central busbar does not permit overlapping of cells for high density packing. Therefore, an improved grid pattern with an edge busbar is desired.

The geometry of fingers themselves is an important consideration in the front contact grid design, since the finger shadowing determines the amount of unavoidable loss. A balance must be obtained between series resistance losses due to reduced geometries and obscuration losses due to increased geometries. After a careful analysis, the method of Scharlack[17] was chosen for finger geometries. This analysis predicts optimum performance with an exponentially narrowing finger geometry. This contact grid designed by this method shown in Fig. 18 consists of an edge busbar and 25 fingers narrowing exponentially from 107 μm (.0042") to 12 μm (.00047"). Since our mask making equipment is limited to generating various shaped rectangles, a 10 step linear approximation was chosen for the exponential curve. A mask set was fabricated with this pattern and the measured obscuration was 5.8%. The actual measured obscuration of an electroplated 2cm x 2cm contact grid was 6.2%. This increase is due to the electroplating process itself as well as broadening due to additional photolithographic steps.

C. Antireflection (AR) Coating

For our GaAs solar cells, we have been using anodic oxide as the AR coating. The refractive index of anodic coating is about 1.83 (Reference 4), and is not optimal, even for one-layer AR coating. For multilayer AR coatings, different coating materials must be used. To find the optimal

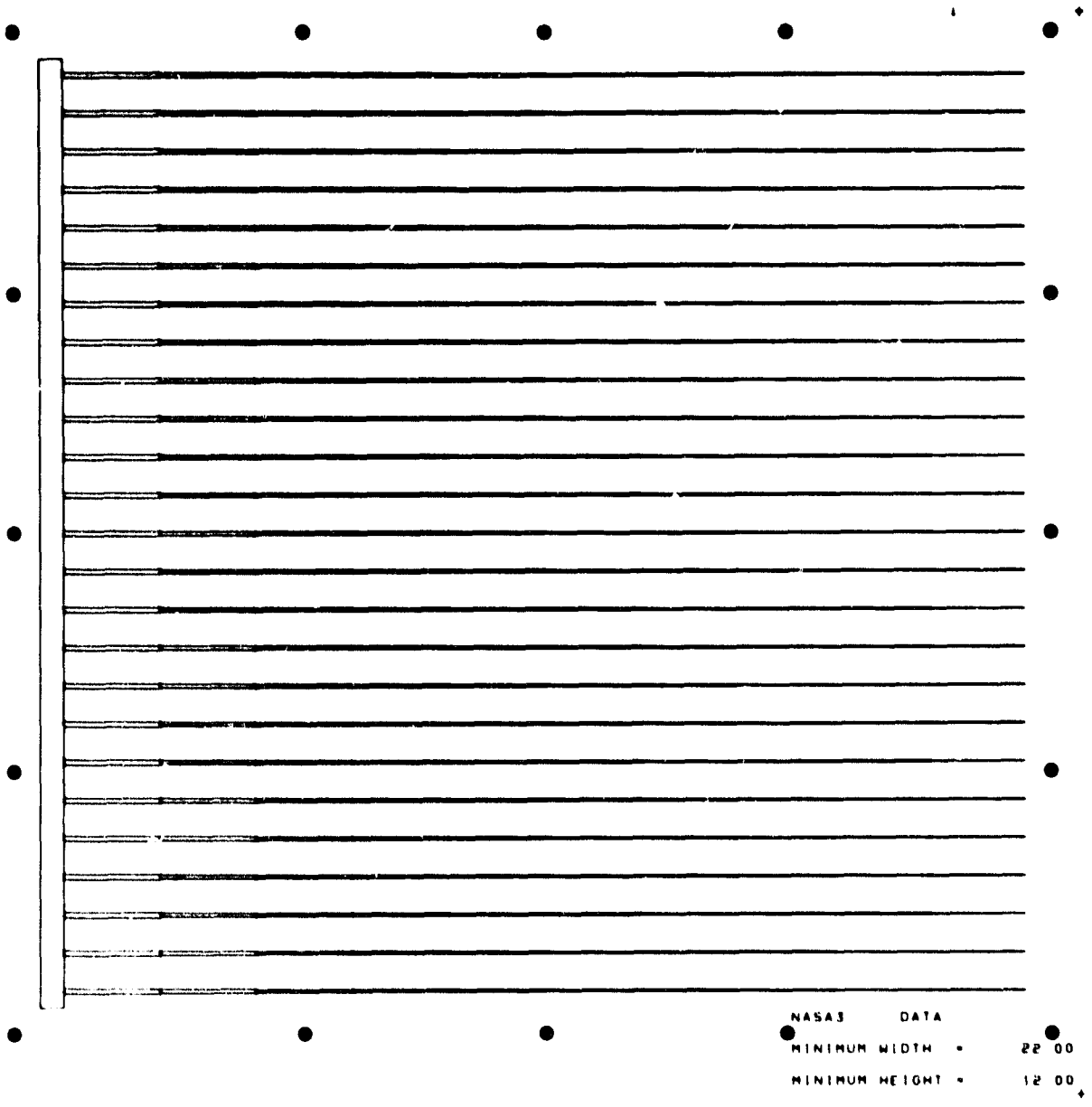


Fig. 18. Schematic diagram of the new front contact mask. Small circular dots at perimeter of mask are contact dots for small test mesa cells.

optical match, we used an existing computer program to predict the optimal thicknesses, and refractive indicies of AR coatings for our GaAs solar cells. The computer model is written such that, once given the measured values of quantum efficiency as a function of wavelength of a cell, the short-circuit current density $J_{SC}$ can be calculated by integrating from 0.35 to 0.90 μm the quantum efficiency values with photon flux of either AM0, AM1 or AM2. The calculated $J_{SC}$ should and does correspond well with the measured current density. Then the measured values of quantum efficiency are modified by have different AR coatings on the cell; thus giving rise to different $J_{SC}$. Given a set of initial conditions, such as the refractive indicies of the two layers for a two-layers AR coating, the computer program will automatically search the optimal conditions (in this case the thicknesses of these two layers), so that the resultant short-circuit current density is maximized for AM0, AM1 or AM2. The computer program has a lot of built-in flexibility. For example, given a particular solar cell, it can predict, for a two-layer AR coating, the optimal refractive indicies, and thicknesses of the two AR materials for the particular desired air mass. The calculations are based on normal incidence.

This computer program provides very interesting conclusion. For our calculcations, we select the measured values of one of our good GaAs solar cells (with conversion efficiency of about 18.5% AM1). The optimization was done for AM0, and for either a single-layer or a double-layer AR coating. Table II shows the results for a single-layer AR coating. Each layer is assumed to have a value of refractive index that is constant over the wavelength range of interest.

TABLE II

CALCULATED AMO SHORT-CIRCUIT CURRENT DENSITY $J_{sc}$ FOR A SHALLOW-HOMOJUNCTION GaAs SOLAR CELLS USING DIFFERENT ONE-LAYER AR COATINGS

| REFRACTIVE INDEX OF AR COATING | OPTIMAL THICKNESS Å | $J_{SC}$ (mA/cm$^2$) |
|---|---|---|
| 1.83 | 825 | 28.421 |
| 1.945 | 777 | 28.510 |
| 2.0 | 747 | 28.492 |
| 2.3 | 635 | 27.849 |

For AR materials such as $SnO_2$, or $In_2O_3$ (refractive index of 2.0), the $J_{sc}$ of a cell coated with such AR coating is about the same as that obtained for a cell coated with anodic oxide. Using a $TiO_2$ AR coating (refractive index of about 2.3) $J_{sc}$ will be significantly decreased. The optimal refractive index is 1.945; however, the increase in $J_{sc}$ is still not significant enough to cause us to change our AR coating from the presently-used anodic oxide coating.

For a double-layer AR coating, the improvement in $J_{sc}$ can be substantial, if proper AR materials are used. The calculations are mainly based on the use of a $MgF_2$ coating as the top layer. The refractive index of our electron-beam evaporated $MgF_2$ is measured to be 1.38. Using this $MgF_2$ layer in conjunction with the anodic coating, our calculation shows that there is no improvement in $J_{sc}$ (see Table III). In fact, it is better that $MgF_2$ is not used at all. There is only a small increase in $J_{sc}$ if a double-layer AR coating is used with top and bottom layers having refractive indicies of 1.38 and 2.0, respectively. A refractive index of 2.3 for the bottom layer will give better results. However, the improvement over a single-layer anodic AR coating is still not very significant. For a $MgF_2$ top AR layer, the optimal bottom layer should have a refractive index of 2.556. Such a double-layer coating is excellent (see Fig. 19) and would give a 5% increase in $J_{sc}$ over our present cell. The computer calculations also show the best double-layer AR coating should have a top layer with a refractive index of 1.505 and a bottom layer of 2.754. All these calculations indicate that unless transparent AR coatings having refractive indicies over 2.3 can be deposited on our GaAs

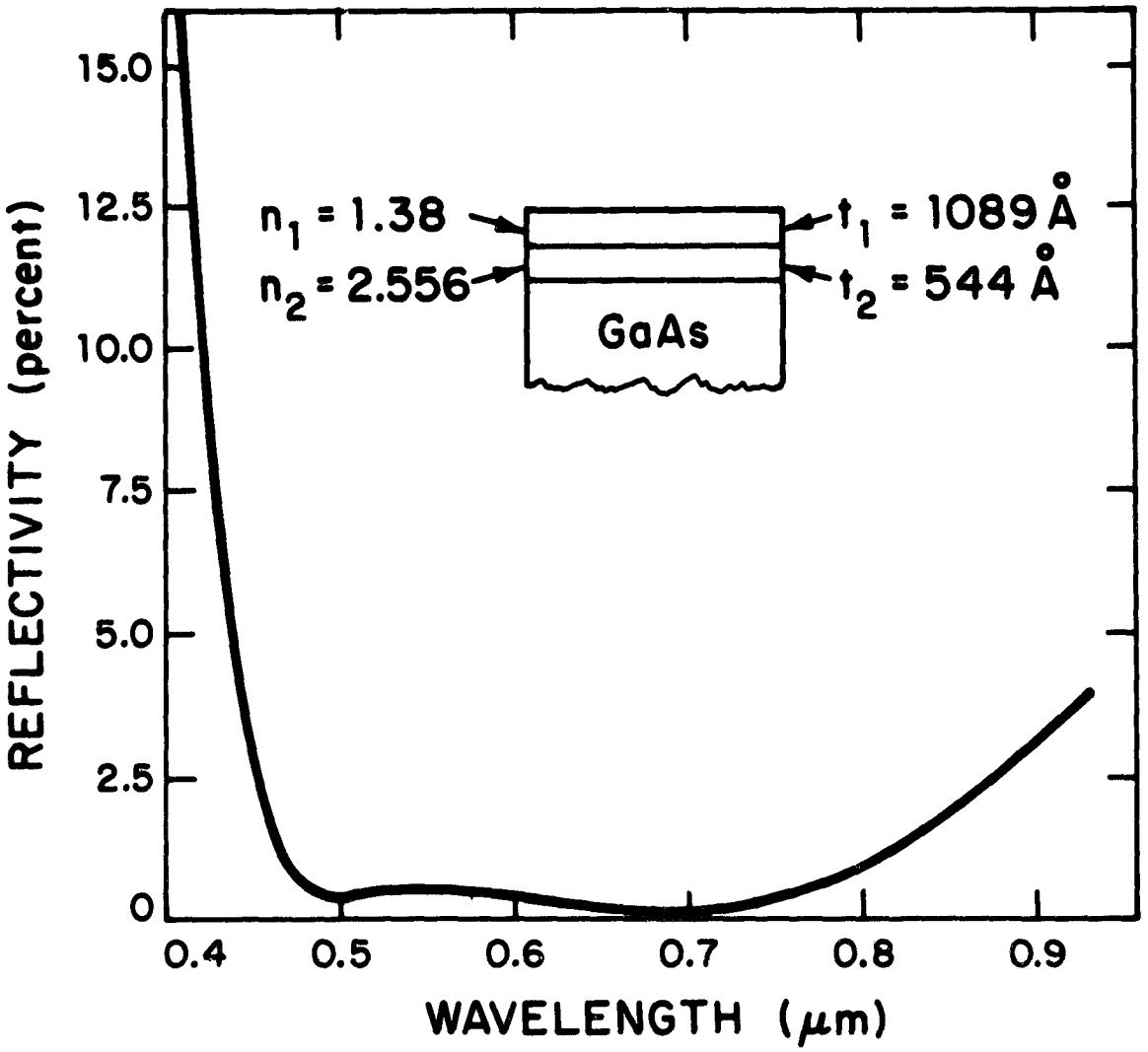


Fig. 19. Calculated reflectivity of a GaAs solar cell using a double-layer AR coating.

TABLE III

CALCULATED AMO SHORT-CIRCUIT CURRENT DENSITY $J_{sc}$ FOR A SHALLOW-HOMOJUNCTION GaAs SOLAR CELLS USING DIFFERENT TWO-LAYER AR COATINGS

| REFRACTIVE INDEX OF TOP AR LAYER | REFRACTIVE INDEX OF BOTTOM AR LAYER | OPTIMAL THICKNESS OF TOP AR LAYER (A) | OPTIMAL THICKNESS OF BOTTOM AR LAYER (A) | $J_{SC}$ ($mA^2/cm^2$) |
|---|---|---|---|---|
| 1.38 | 1.83 | 0 | 825 A | 28.421 |
| 1.38 | 2.0 | 584 | 610 | 28.770 |
| 1.38 | 2.3 | 1034 | 601 | 29.544 |
| 1.38 | 2.556 | 1089 | 544 | 29.826 |
| 1.505 | 2.754 | 1009 | 495 | 29.892 |

cells, it is of no significant advantage to use any AR coating other than our present anodic layer. Since currently we can only deposit (by electron beam evaporation) $Ta_2O_5$ with refractive index of 2.0, we decided to keep using our anodic AR coating. We have, however, explored the plasma deposition of $Si_3N_4$, and have some initial success in obtaining transparent $Si_3N_4$ layers with refractive index of about 2.5. It is conceivably that further development in $Si_3N_4$ may allow us to use efficient double-layer AR coating.

## V. SUMMARY

We have developed a new process in obtaining ultrathin single-crystal GaAs cells, and solar cells of conversion efficiencies as high as 17% AM1 have been fabricated from 10-μm thick GaAs films.

The design and construction of OM CVD system was completed, and this new system is expected to permit us to grow GaAs and III-V ternary compounds for solar cell applications.

## REFERENCES


1. J. C. C. Fan, R. L. Chapman, C. O. Bozler, and P. J. Drevinsky, Appl. Phys. Lett. 36, 53 (1980).
2. J. J. Wysocki and P. Rappaport, J. Appl. Phys. 31, 571 (1960).
3. N. J. Nelson, K. K. Johnson, R. L. Moon, H. Y. Vanderplas, and L. W. James, Appl. Phys. Lett. 33, 26 (1978).
4. J. C. C. Fan, C. O. Bozler and R. L. Chapman, Appl. Phys. Lett. 32, 390 (1978), DDC AD-A058281/7.
5. C. O. Bozler, J. C. C. Fan, and R. W. McClelland, Chapter 5 in Gallium Arsenide and Related Compounds (St. Louis) 1978 (The Institue of Physics, London, 1979), p. 429, DDC AD-A072370/0.
6. J. C. C. Fan, C. O. Bozler and B. J. Palm, Appl. Phys. Lett. 35, 875 (1979), DDC AD-A085501/5.
7. J. M. Woodall and H. J. Hovel, Appl. Phys. Lett. 30, 492 (1977).
8. G. W. Turner, J. C. C. Fan, R. L. Chapman, and R. P. Gale, Proc. Fifteenth Photovoltaic Specialists Conference - 1981, Orlando, Florida, 12-15 May 1981, pp. 151-155.
9. R. P. Gale, J. C. C. Fan, B-Y. Tsaur, G. W. Turner, and F. M. Davis, IEEE Electron Device Lett. EDL-2, 169 (1981).
10. M. Konagai, M. Sagimoto, and K. Takashi, J. Cryst. Growth 45, 277 (1978).
11. R. W. McClelland, C. O. Bozler, and J. C. C. Fan, Appl. Phys. Lett. 37, 560 (1980).

12. C. O. Bozler, R. W. McClelland, and J. C. C. Fan, Proceedings of 8th International Symposium on GaAs and Related Compounds (Vienna) 1980 (Institute of Physics, London, 1981), p. 283.

13. C. O. Bozler, R. W. McClelland, and J. C. C. Fan, IEEE Electron Device Lett. EDL-2, 203 (1981).

14. Final Report, "Gallium, Long-Term Supply," prepared for the Solar Energy Research Institute by Charles River Associate, Boston, MA, Report No. CPA483 (June 1980).

15. J. C. C. Fan, C. O. Bozler, and R. W. McClelland, Proc. Fifteenth IEEE Photovoltaic Specialists Conference - 1981, Orlando, Florida, 12-15 May 1981, pp. 666-672.

16. Final Report "GaAs Shallow-Homojunction Solar Cells," NASA CR-165167, Lincoln Laboratory, M.I.T. (30 June 1980).

17. R. S. Scharlack, Solar Energy 23, 199 (1979).